# Hydrogen adsorption on $RuO_2(110)$: Density-functional calculations

Qiang Sun, Karsten Reuter, and Matthias Scheffler
*Fritz-Haber-Institut der Max-Planck-Gesellschaft, Faradayweg 4-6, D-14195 Berlin-Dahlem, Germany*
(Received 17 September 2003; revised manuscript received 19 August 2004; published 2 December 2004)

The structural, vibrational, energetic, and electronic properties of hydrogen at the stoichiometric $RuO_2(110)$ termination are studied using density-functional theory. The oxide surface is found to bind both molecular and dissociated $H_2$. Apart from the most stable configuration in the form of hydroxyl groups (monohydrides) at the undercoordinated $O^{br}$ surface anions, we also identify a molecular state at the undercoordinated $Ru^{cus}$ atoms (dihydrogen) and a waterlike species (dihydride) at the $O^{br}$ sites. Hydrogen adsorption at $O^{br}$ sites increases the reactivity of the neighboring $Ru^{cus}$ sites, which are believed to play a key role in catalytic oxidation reactions.

DOI: 10.1103/PhysRevB.70.235402 PACS number(s): 68.47.Gh, 68.43.Bc, 68.43.Pq, 82.65.+r

## I. INTRODUCTION

The widespread use of transition metal (TM) oxides, for example, in applications for catalysis, electrochemistry, gas sensors, and corrosion/wear protection is an increasing source of motivation for fundamental research on this material class. An important goal in such studies, focusing on the surface functionality of oxides, is to establish atomic-scale insight into their surface structure and composition, as well as their interaction with gas phase species.[1,2] Despite notable efforts secure knowledge is still rather scarce. This holds even for well-defined single-crystal surfaces under the controlled conditions of ultrahigh vacuum (UHV), mostly due to the structural complexity of oxides and to their often insulating nature which hampers the use of electron spectroscopies.[3]

With respect to these issues crystalline $RuO_2$ represents a good choice for a benchmark model system. It is one of the few conducting TM oxides and its rutile bulk structure is of modest complexity.[4] This makes studying this system feasible, but with, e.g., a reported high catalytic activity in oxidation reactions[5–7] and being discussed as playing a sensitive role in Pt-Ru based direct methanol fuel cells,[8] it is also sufficiently interesting from an applied perspective. Especially the low energy $RuO_2(110)$ surface has recently received particular attention.[6,7,9–16] Focusing mostly on the CO oxidation reaction quite some detailed understanding (experimental as well as theoretical) on the fundamental interaction of O and CO with this model surface has emerged from these studies.

From the potential interest for both catalytic and fuel cell applications it now appears natural to extend this knowledge also to the interaction of hydrogen with $RuO_2(110)$. From a chemical point of view this ubiquitous gas phase species is expected to form strong bonds particularly with the oxygen anions at the oxide surface.[2] Intentionally or unnoticed, adsorbed hydrogen could therefore be present as surface species in a wide range of conditions, significantly influencing the functionality in the targeted application. In fact, a noticeable effect of hydrogen contamination on the CO turnover numbers has already been discussed in a recent experimental study.[17]

On a microscopic level Wang *et al.* have provided detailed kinetic and vibrational experimental data on the low-temperature hydrogen adsorption at $RuO_2(110)$ in UHV.[18] Using high-resolution electron energy-loss spectroscopy (HREELS) and temperature programmed desorption (TPD) they identified both a molecular and a dissociated hydrogen state, the latter exhibiting vibrational properties of a waterlike species with, however, a peculiarly blueshifted scissor mode. Motivated by these results and as a first step towards an understanding of hydrogen interaction with this surface, we set out to investigate the structural, vibrational, energetic, and electronic properties of possible H adsorption sites at the stoichiometric $RuO_2(110)$ surface using density-functional theory (DFT).[19] The stability of molecular and dissociated hydrogen is first discussed at either of the two prominent adsorption sites exhibited by this oxide surface (Secs. IV A and IV B). Then higher coverages involving simultaneous occupation of both sites are addressed (Sec. IV C). Combining these static results with the detailed experimental data provided from the HREELS and TPD study of Wang and co-workers, one may even tentatively discuss some aspects of the intricate low temperature dissociation kinetics of $H_2$ at this surface, as has been done briefly in a preceding communication.[18]

## II. COMPUTATIONAL DETAILS

The DFT calculations were performed within the full-potential linear augmented plane wave (FP-LAPW) method[20–22] using the generalized gradient approximation (GGA)[23] for the exchange-correlation functional. The FP-LAPW basis-set parameters are as follows: $R_{MT}^{Ru}=1.8$ bohr, $R_{MT}^{O}=1.0$ bohr, $R_{MT}^{H}=0.6$ bohr, $E_{max}^{wf}=20.25$ Ry, $E_{max}^{pot}=400$ Ry, wave-function expansion inside the muffin tins up to $l_{max}^{wf}=12$, and potential expansion up to $l_{max}^{pot}=6$. The Ru 4*s* and 4*p*, as well as the O 2*s* orbitals were treated as valence states, adding corresponding local orbitals to the LAPW basis set. The Brillouin zone integration employed a $(4\times9\times1)$ Monkhorst-Pack grid for $(1\times1)$ surface unit-cells, a $(4\times4\times1)$ grid for $(1\times2)$ cells, and a $(5\times5\times8)$ grid for the bulk calculations.

We stress that the very short O—H bonds represent a formidable challenge to electronic structure theory calculations in general. With respect to the FP-LAPW method employed this translates into the necessity to use rather small nontouching muffin-tin spheres. Then, the convergence be-

 

havior with respect to the interstitial plane wave cutoff is rather slow, requiring one to use much higher $E_{max}^{wf}$ than the ~17–19 Ry typical for late TM oxide studies involving muffin-tin sphere sizes only dictated by the O-metal bonds. Correspondingly, we tested this convergence by increasing the plane wave cutoff up to 36 Ry (!), as well as by doubling our k-mesh density. From these detailed tests (cf. the Appendix), we conclude that the structural properties of the systems addressed in the present study are well converged within 0.02 Å in bond lengths and 6° in bond angles at the above stated $E_{max}^{wf}=20.25$ Ry, which correspondingly was chosen as our standard cutoff. Relative binding energy *differences* between configurations involving the same number of O and H atoms (e.g., when comparing tilted and untilted geometries) appear similarly well converged to within 0.05 eV at this cutoff. For absolute H binding energies on the other hand, in particular when they involve strong O—H bonds like in hydroxyl groups, the chosen, already rather high cutoff is, however, still not sufficient. Where such numbers were required within a 0.1 eV/H atom numerical accuracy for our physical argument and are then listed in this paper, we correspondingly ran subsequent calculations at a very (for routine calculations still prohibitively) high cutoff of $E_{max}^{wf}=30$ Ry employing the structure relaxed before at $E_{max}^{wf}=20.25$ Ry. While already these numerical uncertainties due to basis sets that are presently feasible for such complex oxide surface calculations dictate a very careful and cautious proceeding, one has additionally to be aware of the general imprecision introduced by the approximate exchange-correlation functional employed in the DFT calculations. To this end, we performed a number of calculations employing also the local-density approximation (LDA)[24] and will comment on the differences between results obtained within LDA and GGA below.

The $RuO_2$(110) surface was modeled by a three trilayer O—($Ru_2O_2$)—O periodic slab as detailed before,[12,13] using a vacuum region of about 13 Å to decouple the interactions between neighboring slabs in the supercell geometry. All structures were fully relaxed by a damped Newton scheme until the residual forces on the atoms were less than 50 meV/Å, keeping only the atomic positions in the central trilayer at their fixed bulk positions. Test calculations employing 5 and 7 trilayer slabs and relaxing also deeper lying layers showed no significant structural changes beyond the topmost trilayer, neither was there an influence on the atomic surface geometries as obtained with the three trilayer calculations. At this point we would further like to emphasize that the structural relaxation allowed for any symmetry breaking at the surface. This was found to be crucial to obtain the correct energetics and structures, which often involve significant tilting of the surface functional groups.

For the calculations of the vibrational modes of the various surface species, the dynamical matrix was set up by displacing each of the involved surface atoms from their equilibrium positions in 0.04 Å steps. Anticipating a good decoupling of the vibrational modes due to the large mass difference between Ru and O/H, the positions of all atoms in the substrate below the adsorption site were kept fixed in these calculations. The normal modes were then obtained by subsequent diagonalization of the dynamic matrix.

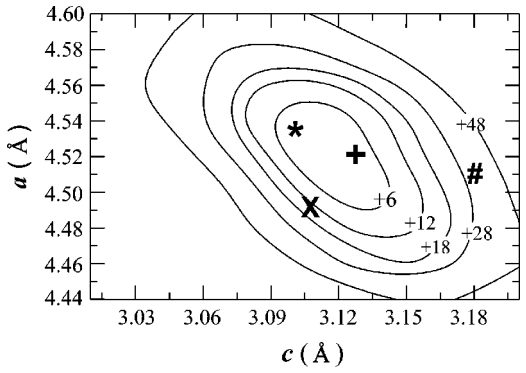


FIG. 1. Computed GGA energy contours as a function of $RuO_2$ bulk lattice parameters $a$ and $c$ (with optimized internal parameter $u$). The energy zero corresponds to the optimized values of $a=4.52$ Å and $c=3.13$ Å marked with "+" and higher contour levels are labeled in the figure in meV per $RuO_2$ formula unit. Additionally shown are the bulk lattice parameters as determined by experiments [* (Ref. 9), × (Ref. 27), and # (Ref. 28)]. The bulk lattice parameters obtained by an earlier DFT-GGA pseudopotential study are $a=4.65$ Å and $c=3.23$ Å (Ref. 9), outside of the range shown in the figure.

## III. BULK $RuO_2$, CLEAN (110) SURFACE, FREE $H_2$ AND $H_2O$

Summarizing and extending the results of our earlier publications on $RuO_2$,[12–16] we first briefly describe the calculated properties of the bulk and the clean (110) surface, as well as free $H_2$ and $H_2O$ molecules, as far as they are relevant for the understanding of the hydrogenated surface discussed below.

$RuO_2$ crystallizes in the rutile structure, described by lattice parameters $a$ and $c$, as well as one internal degree of freedom $u$ specifying the positions of the O anions within the bulk unit cell.[4] In order to determine the bulk equilibrium lattice constants we scanned a grid in $a$ and $c$ near the experimental values with 0.02 and 0.015 Å steps, respectively, both at our standard (20.25 Ry) and at a high interstitial plane wave cutoff (30 Ry). At each grid point the internal parameter $u$ was further optimized minimizing the computed forces on the O atoms in the unit cell. The resulting energy landscapes were almost identical for both cutoffs and we show in Fig. 1 the results at the higher cutoff, while Table I lists the determined bulk lattice parameters within the LDA and GGA. Comparing with available bulk diffraction studies[26,27] we obtain very good agreement within the GGA. Interestingly, two earlier DFT pesudopotential calculations (LDA[25] and GGA[9]) yield larger lattice parameters that deviate by more than 0.1 Å from our LDA and GGA values, respectively. We particularly checked on the GGA value by Kim *et al.*,[9] but find their geometry to be about 0.4 eV per $RuO_2$ formula unit higher in energy than our ground state geometry. Finally, we notice that the $c$ lattice parameter measured in two independent low-energy electron diffraction (LEED) experiments[9,28] deviates from the bulk diffraction results by about 0.1 Å. In both LEED experiments thin $RuO_2$(110) films grown on Ru(0001) were investigated, where the $c$ lattice parameter corresponds to the size of the surface-unit cell in the [001] direction. Apparently, a thin

TABLE I. $RuO_2$ lattice constants ($a$, $c$, and $u$) and bulk modulus ($B_0$) as determined within LDA and GGA, full-potential (FP) and pseudopotential (PP) calculations. Experimental values are from x-ray diffraction (XRD) and low-energy electron diffraction (LEED) experiments.

| | $a$ (Å) | $c$ (Å) | $u$ | $B_0$ (GPa) |
|---|---|---|---|---|
| This work (FP-LDA) | 4.42 | 3.05 | 0.306 | 352 |
| This work (FP-GGA) | 4.52 | 3.13 | 0.306 | 294 |
| Reference 25 (PP-LDA) | 4.56 | 3.16 | 0.307 | 283 |
| Reference 9 (PP-GGA) | 4.65 | 3.23 | 0.305 | |
| Reference 26 (XRD) | 4.492 | 3.106 | 0.306 | 270 |
| Reference 27 (XRD) | 4.491 | 3.106 | | |
| Reference 28 (LEED) | 4.51 | 3.18 | | |
| Reference 9 (LEED) | 4.51 | 3.23 | | |

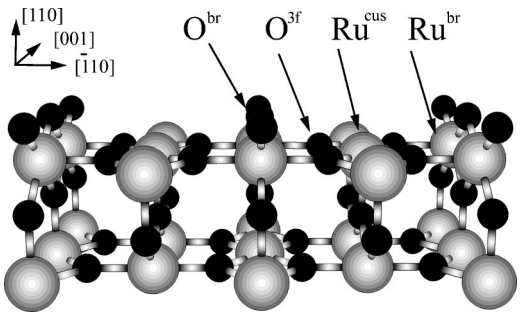


FIG. 2. Side view of the stoichiometric $RuO_2$(110) surface termination explaining the location of the two prominent adsorption sites corresponding to undercoordinated surface atoms: bridging oxygen $O^{br}$ and coordinatively unsaturated (cus) ruthenium $Ru^{cus}$ (Ru=light, large spheres; O=dark, small spheres).

film (with an incommensurable structure to that of the metal substrate) prefers a slightly different geometry than a bulk crystal.

Depending on the oxygen-content in the surrounding gas phase, either a stoichiometric or an oxygen-rich termination is stabilized at the $RuO_2$(110) surface.[12,16] Figure 2 shows the surface geometry of the stoichiometric termination exhibiting two kinds of surface species, the nearest neighbor shell of which has been reduced by the creation of the surface: A twofold coordinated bridging oxygen $O^{br}$ (threefold coordinated in the bulk) and a fivefold coordinated ruthenium atom $Ru^{cus}$ (sixfold coordinated in the bulk). The only other surface species present, $O^{3f}$, still maintains its bulklike threefold coordination to in-plane Ru atoms. The oxygen-rich termination differs from this geometry only by extra oxygen atoms adsorbed on top of the $Ru^{cus}$ atoms. In the following we will focus exclusively on the interaction of hydrogen with the stoichiometric termination, attempting to make contact with the existing data from ultrahigh vacuum (UHV) experiments,[18] where the stoichiometric termination is the standard surface produced after a high-temperature anneal to 600 K.[6,9–11] The discussion of hydrogen interaction with the oxygen-rich termination is deferred to a consecutive publication.

Due to the cutting of bonds the surface atoms relax. Most prominently we find that the $O^{br}$ atoms move inward, reducing their bond length to the underlying Ru atoms (henceforth denoted $Ru^{br}$) to 1.91 Å (bulk: 1.99 Å), and, correspondingly, the interlayer distance is reduced to 1.09 Å (12% smaller than bulk). These findings are in very good agreement with a recent LEED study which determined a bond length of 1.94 Å and a first layer contraction of −13% at $RuO_2$(110),[9] and they are similar to the geometric changes observed at the isostructural $TiO_2$(110) surface.[29] Although not as pronounced, also the under-coordinated $Ru^{cus}$ atoms relax a bit inwards, thereby inducing a buckling within the first trilayer plane of 0.16 Å (LEED: 0.18 Å). Contrary to other transition metal oxide surfaces like, e.g., $Al_2O_3$(0001)[30] the structural relaxations are therefore rather small, and in particular damp away rapidly: No significant deviations from the bulklike positions are found for atoms below the first trilayer, neither in LEED, nor in our thicker slab test calculations.

Finally, we summarize in Table II the computed binding energies, bond lengths, and frequencies for gas phase $H_2$ and $H_2O$. For the binding energies we also needed the total energies of atomic O and H. For both the molecular and atomic calculations we employed the same muffin-tin spheres as detailed before for the slab calculations. We furthermore made sure that symmetry constraints would not impose an artificial higher energy configuration with fractional occupation of the eigenlevels. The total energies for the isolated, spin-polarized atoms are obtained by adding to the total energy value from a non-spin-polarized FP-LAPW calculation a constant spin-polarization energy of 1.52 eV (O) and 1.10 eV (H) taken from a relativistic atomic DFT calculation for spherical atoms.[20,34] With respect to structural and vibrational properties we obtain very good agreement with the experimental data, as well as with previous DFT studies.[35–38] While the geometries are well converged already at 20.25 Ry, the slow convergence of the O—H bond energetics already described in the preceding section is also well apparent for the free $H_2O$ molecule, which is why we list the computed values both at the routine 20.25 Ry and at the very high LAPW cutoffs of 30 Ry and 36 Ry. The 30 Ry cutoff is used later on to obtain quantitative binding energies at the surface as discussed above.

With respect to the 36 Ry cutoff we assess the numerical convergence of the gas phase binding energies to be within 0.1 eV. This points then at some error (i.e., overbinding) compared to the experimental values when oxygen is involved even within the GGA, which is a well-known result.[23] Although some error cancellation could occur in the computation of binding energies at surfaces, we conclude that a cautious reasoning is necessary when judging on the endo- or exothermicity of adsorption with respect to the gas phase molecules. To this extent, we stress that all corresponding conclusions below refer only to the explicit GGA functional used. In most cases, the numbers are such that they appear outside the uncertainty range of current gradient-corrected functionals, but a real verification would require higher level calculations, which are unfortunately at present prohibitive for such complex surface systems.

TABLE II. Structure parameters (bond length $d$ in Å and angle in deg), binding energy $E_b$ (in eV), and vibrational frequencies $\nu$ (in meV) for gas phase $H_2$ and $H_2O$. Compared are the computed values for LDA and GGA (at two different LAPW cutoffs) with the corresponding experimental data (with zero-point energy removed).

| | LDA | | | GGA | | | |
|---|---|---|---|---|---|---|---|
| Cutoff (Ry) | 20.25 | 30 | 36 | 20.25 | 30 | 36 | Experiment |
| $H_2$ | | | | | | | |
| $d_{H—H}$ | 0.77 | 0.77 | 0.77 | 0.75 | 0.75 | 0.75 | 0.74 (Ref. 31) |
| $E_b$ | 4.79 | 4.87 | 4.88 | 4.45 | 4.56 | 4.57 | 4.73 (Ref. 31) |
| $\nu_{stretch}$ | | | | 538 | | | 546 (Ref. 32) |
| $H_2O$ | | | | | | | |
| $d_{O—H}$ | 0.98 | 0.98 | 0.97 | 0.97 | 0.97 | 0.97 | 0.96 (Ref. 32) |
| $\angle_{HOH}$ | 102 | 102 | 103 | 103 | 103 | 102 | 104.5 (Ref. 32) |
| $E_b$ | 10.71 | 11.12 | 11.16 | 9.67 | 10.03 | 10.15 | 10.06 (Ref. 33) |
| $\nu_{sym}$ | | | | 424 | | | 454 (Ref. 32) |
| $\nu_{asym}$ | | | | 435 | | | 466 (Ref. 32) |
| $\nu_{scissor}$ | | | | 189 | | | 198 (Ref. 32) |

## IV. THE HYDROGENATED $RuO_2$(110) SURFACE

In the following sections we discuss the hydrogen interaction with the various surface species present at the stoichiometric $RuO_2$(110) termination. The energetics will be described with respect to the free $H_2$ molecule, where a negative binding energy denotes endothermicity with respect to the gas phase species and the bare surface, i.e., a metastable situation. As we find the interaction with the threefold coordinated in-plane $O^{3f}$ to be energetically very unfavorable (even the formation of a monohydride is endothermal by $\approx -0.3$ eV/H atom), the discussion will concentrate on the two undercoordinated surface species, i.e., $Ru^{cus}$ and $O^{br}$. At first we discuss hydrogen to be present at one of these sites only (Secs. IV A and IV B); and then we consider simultaneous adsorption at both sites (Sec. IV C). Consistent with our previous publications we will employ a shorthand notation to characterize the manyfold of studied geometries, indicating first the occupancy of the bridge site and then of the cus site, e.g., $(OH)^{br}/H_2^{cus}$ for a configuration with an OH-group at the bridge site and a $H_2$ molecule at the cus site.

Lateral interactions between functional groups at directly neighboring cus and bridge sites are implicitly contained within our calculations employing $(1\times1)$ surface unit cells. With these cells only integer multiples of one monolayer (ML) hydrogen coverage can be studied [1 ML defined as monoatomic occupation of all sites of one type (br or cus)]. Further reaching lateral interactions, e.g., towards a moiety at the same site type either along $[\bar{1}10]$ (at a distance of 6.4 Å) or along [001] (at a distance of 3.1 Å, see Fig. 3) could lead to the formation of more dilute superstructures with fractional MLs hydrogen coverage. From a systematic study of oxygen adsorption at $RuO_2$(110) we find such lateral interactions to be below 0.1 eV between sites more than 6 Å away at this rather open oxide surface.[39] We do not expect this to be significantly different for hydrogen, in particular along the longer $[\bar{1}10]$ direction of the surface unit cell, where the next-nearest site would be 6.4 Å away. Correspondingly, we only test for lateral interactions in selected configurations employing larger $(1\times2)$ cells, allowing us to model structures where then only every second site (at 6.2 Å distance) is occupied along the [001] direction (see, e.g., Fig. 7 below).

### A. Hydrogen at $Ru^{cus}$

We start with the molecular adsorption of $H_2$ at the undercoordinated $Ru^{cus}$ site ($O^{br}/H_2^{cus}$). This analysis was motivated by the aforementioned recent UHV HREELS experiments that attributed a weak peak at 367 meV to the stretch mode of a molecular hydrogen species at the surface with a TPD activation energy of about 0.3 eV.[18] Relaxing a $H_2$ molecule in $(1\times1)$ cells from a height at about 2 Å atop the cus sites our calculations indeed find such a (meta)stable species with a computed binding energy of +0.32 eV/$H_2$ with respect to molecular $H_2$. The resulting adsorption geometry is shown in Fig. 3 together with the calculated vibrational modes. At a height of 1.85 Å the $H_2$ molecule lies parallel to the surface above the cus sites (side-on configuration). Interestingly, we find almost no corrugation of the potential energy surface with respect to an azimuthal rotation of the flat-lying $H_2$ molecule: The optimal bond orientation about 30° from the $[\bar{1}10]$ direction is only by insignificant 3 meV more stable than any other orientation, i.e., the $H_2$ behaves essentially like a free-rotator (helicopter mode), as also reflected by the very low rotational vibration frequency of 12 meV, cf. Fig. 3. The similarly low in-plane translational modes further point at a rather expressed delocalization of the $H_2$ molecule parallel to the surface, particularly in the $[\bar{1}10]$ direction, i.e., approaching the neighboring bridging oxygens. Despite this, the $H_2$ bond length is with 0.81 Å noticeably stretched com-

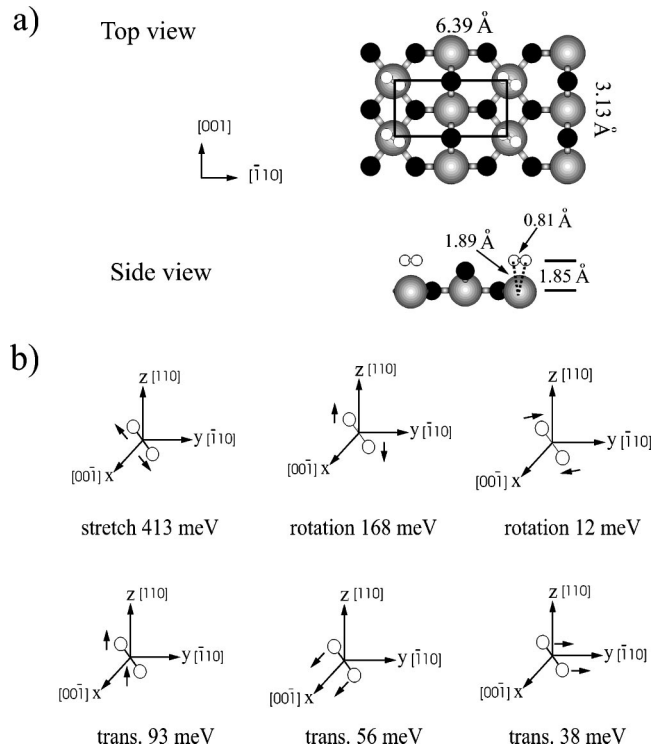


FIG. 3. (a) Top and side view of the adsorption geometry of 1 ML $H_2$ at $Ru^{cus}$ (Ru=light, large spheres; O=dark, small spheres; and H=white, small spheres). Additionally shown is the size of the $(1\times1)$ surface unit cell. Note that the azimuthal direction of the plotted $H_2$ is arbitrary, as it is freely rotating. (b) Six vibrational modes of the adsorbed $H_2$ molecule. The directions and lengths of the arrows indicate approximately the directions and relative magnitudes of the displacements of the atoms.

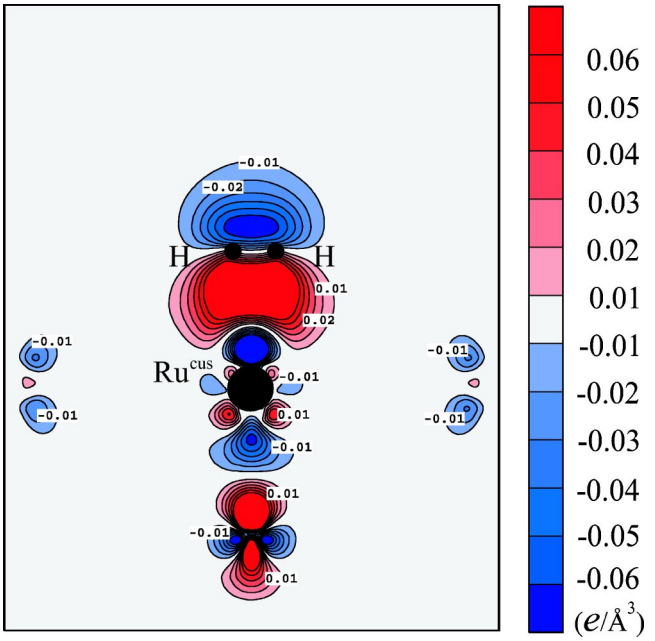


FIG. 4. Difference density plot for $H_2$ adsorbed at $Ru^{cus}$. The contour plot depicts the plane parallel to the $H_2$ molecular axis and normal to the surface. Areas of electron accumulation and depletion have positive and negative signs, respectively, contour lines are drawn at 0.01 $e/Å^3$ intervals.

pared to the free gas phase molecule (0.75 Å). This is consistent with the rather high binding energy and the significantly decreased stretch vibration (413 meV compared to 538 meV in the gas phase).

These properties reflecting a moderate interaction are very similar to molecular $H_2$ at late transition metal surfaces [like, e.g., Pd(100)[40]], if adsorption is restricted to take place at the on-top site. Of course, at the latter surfaces the on-top site is not even a local minimum and $H_2$ would dissociate towards higher-coordinated hollow sites. The different geometry of $RuO_2$(110) does not offer such sites, and thus stabilizes the molecular adsorption at $Ru^{cus}$. In this respect we attribute the nondissociative interaction of $H_2$ with these sites more to a geometry effect, rather than to an electronic effect, i.e., compared with the weak physisorption of $H_2$ at noble metal surfaces like Ag(111).[41]

The relatively strong interaction (electron polarization and bond formation) is also obvious in the "difference density" plot shown in Fig. 4. The "difference density" is obtained by subtracting from the electron density of the adsorbate system that of the clean surface and that of the free molecule (the latter two with the same interatomic distances as found for the adsorbate system).[42] A rather strong polarization of the flat-lying $H_2$ is apparent, with electron density accumulation on the substrate side of the molecule and depletion on the vacuum side. Due to the interaction with the $H_2$ the backbond of the $Ru^{cus}$ atom to the underlying O substrate atom is slightly weakened, the Ru atom moves 0.03 Å upwards and thereby reduces the clean-surface-buckling in the topmost trilayer.

The structure and symmetry of the difference density plot suggests the major interaction in the occupied states to be due to a hybridization of Ru-$d_{z^2}$ and $H_2$-$\sigma$ orbitals. Analyzing the computed local density of states we indeed find the bonding governed by this and a smaller hybridization of the Ru-$d_{xz}/d_{yz}$ with the $H_2$-$\sigma^*$ orbitals. The bonding of the $H_2$ molecule to the cus site can therefore be understood within the familiar donation/backdonation picture,[42] where the hybridization with the $H_2$-$\sigma$ orbital causes a small $H_2\rightarrow$Ru charge transfer that is counteracted by some backdonation of electronic charge from the metal to the $H_2$-$\sigma^*$ level, strengthening the coupling to the substrate while weakening and elongating the H—H bond.

Contrary to the situation at most, more reactive TM surfaces this backdonation is, however, not strong enough to dissociate the $H_2$ molecule. This is supplemented by the surprising result that atomic hydrogen is not stable at the $Ru^{cus}$ site: We compute an endothermal binding energy of $-0.33$ eV/H atom with respect to $1/2\,H_2$ at 1 ML H-coverage, i.e., in $(1\times1)$ unit cells. Checking whether H bonding might become more favorable in more dilute superstructures we also employed $(1\times2)$ cells to model a 0.5 ML H-coverage with H only at every second site along the [001] direction. However, with $-0.20$ eV/H atom with respect to $1/2\,H_2$ the binding energy is still endothermal. Since we expect no further strong changes in binding energy for even more dilute H-phases, where neighboring molecules are then

always further than 6 Å away, we conclude that only molecular hydrogen may be stabilized at the cus sites.

Forming the basis for, e.g., relations between heterogeneous and homogeneous catalysis it is interesting to compare these findings for the Ru atom at the surface of an oxide with the hydrogen bonding to TM atoms in other frameworks like, e.g., at the surface of metals or in a TM complex. As already mentioned, coupling of hydrogen to TM surfaces is generally associated with $H_2$ dissociation.[43] The observation of nondissociative chemisorption of $H_2$ has so far been restricted to a few exceptional cases,[44,45] mostly connected with a prior saturation of the most reactive sites at the surface with atomic hydrogen. Concomitantly, we computed the bonding of atomic H at Ru(0001) to be exothermic at least up to 1 ML coverage. Molecular precursors have more been identified at noble surfaces like Ag(111),[41] yet then physisorbed and certainly not exhibiting such a strong bond elongation and downshift of the stretch frequency as found at $RuO_2$(110). The latter findings resemble much more the data from organometallic complexes: For so-called $\eta^2$-$H_2$ (dihydrogen) single metal atom complexes, in which the H—H bond remains intact,[46] TM-$H_2$ bond energies in the range of 0.1–0.3 eV/$H_2$ are estimated,[47] significant redshifts of the stretch frequency[47,48] and bond elongation up to 0.9 Å are reported.[49,50] In fact, neutron scattering experiments furthermore indicate rapid rotation of $\eta^2$-$H_2$ ligands with an activation energy of less than about 10 meV,[49] just as we find for the molecular hydrogen at $Ru^{cus}$. Even the donation/backdonation bonding model is analogously discussed for the TM complexes.[51] Yet, there (just like at TM surfaces) the backdonation may also break the H—H bond, and often $H_2$- as well as H-ligands are attached to the same metal center and can even exhibit continuous changes between both configurations.[47,48] At $RuO_2$(110), in contrast, the bonding to the surrounding oxide apparently depletes the electron density at the undercoordinated $Ru^{cus}$ atom already in such a way that the back-bonding only weakens the $H_2$ bond, but no longer breaks it.

### B. Hydrogen at $O^{br}$

For $H_2$ molecules approaching the $RuO_2$ surface at the undercoordinated $O^{br}$ atoms we find that they will either slide towards the $Ru^{cus}$ sites or that they are repelled into the gas phase. In no case [i.e., testing many $H_2$ orientations, as well as lower coverages in a $(1\times2)$ cell] did we observe spontaneous dissociation above the $O^{br}$ site. This leads us to conclude that molecular adsorption primarily takes place over the aforediscussed cus sites. Atomic hydrogen, on the other hand, binds at the $O^{br}$ sites, i.e., forming a surface hydroxyl group. The optimized geometry of the 1 ML $(OH)^{br}$/− phase computed in $(1\times1)$ cells is shown in Fig. 5. The strong binding within the OH-group weakens the bond to the underlying $Ru^{br}$ substrate atoms and elongates it significantly from 1.91 to 2.06 Å. The surface OH-group itself has a bond length of 0.97 Å, nearly identical to the O-H distance in $H_2O$, and is inclined towards the $[\bar{1}10]$ direction with a 40° angle with respect to the surface normal. The computed binding energy is +0.89 eV/H atom stronger than

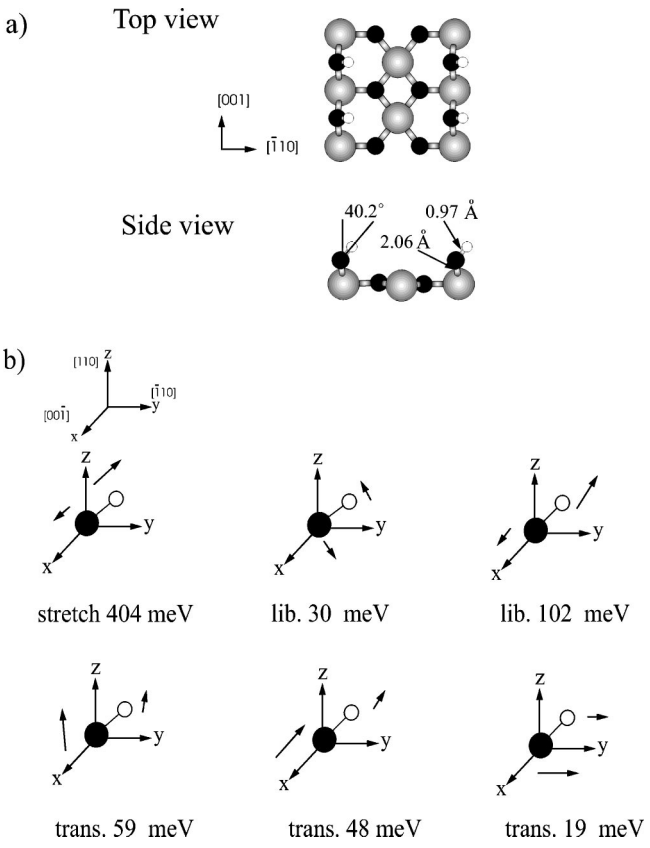


FIG. 5. (a) Top and side view of the adsorption geometry of 1 ML H at $O^{br}$, computed in $(1\times1)$ unit cells. (b) Six vibrational modes of the formed hydroxyl group.

in molecular $H_2$, and the energy gain by the tilting is 0.1 eV/H atom compared to the higher-symmetry, up-right configuration. Again, both the computed stretch frequency, as well as the binding energy, are found to be in good agreement with the recent HREELS and TPD data from the hydroxylated surface,[18] and the strong binding is also nicely visible in the difference density plot shown in Fig. 6.

With only a 0.1 eV energy difference between the tilted and upright position, the hydroxyl groups will at finite temperatures frequently swing from one orientation to the other. Checking whether this may occur in concerted wavelike motions along a chain of bridge sites, we repeated the calculation with 1 ML coverage, but now in a $(1\times2)$ cell with each OH-group alternatingly tilted in one or the other direction as shown in Fig. 7(a). The only structural difference obtained is a somewhat larger tilt angle of about 60°, while bond length and binding energy remain to within 0.01 eV/H atom virtually unchanged. Testing for further reaching lateral interactions by decreasing the total coverage to 0.5 ML as shown in Fig. 7(b), we again find the binding energy within 0.02 eV/H atom degenerate to the previous two cases, leading us to conclude that each OH-group tilts and swings essentially independent of the others and of the total coverage, which may thus easily reach the full 1 ML with each $O^{br}$ atom hydroxylated.

The low temperature HREELS and TPD experiments by Wang *et al.*[18] show that the coverage of dissociated hydrogen can be increased above 1 ML. There is evidence for a hydro-

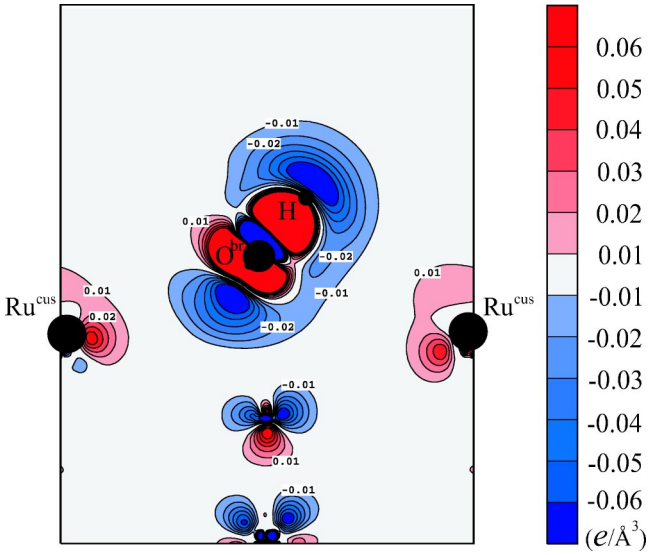


FIG. 6. Difference density plot of a hydroxyl group at the bridge sites $(OH)^{br}/-$. The contour plot depicts the plane parallel to $[\bar{1}10]$ and normal to the surface. Areas of electron accumulation and depletion have positive and negative signs, respectively, contour lines are drawn at 0.01 $e/Å^3$ intervals.

gen state at $O^{br}$ that exhibits frequencies resembling a waterlike H—O—H configuration, i.e., with two H atoms per bridge site (dihydride). Surprisingly, the measured scissor mode for this functional group is 231 meV higher than the one of gas phase water (exp: 198 meV, calc: 189 meV, see Table II), whereas intuitively a redshift would be expected: Considering that the molecule-surface interaction weakens

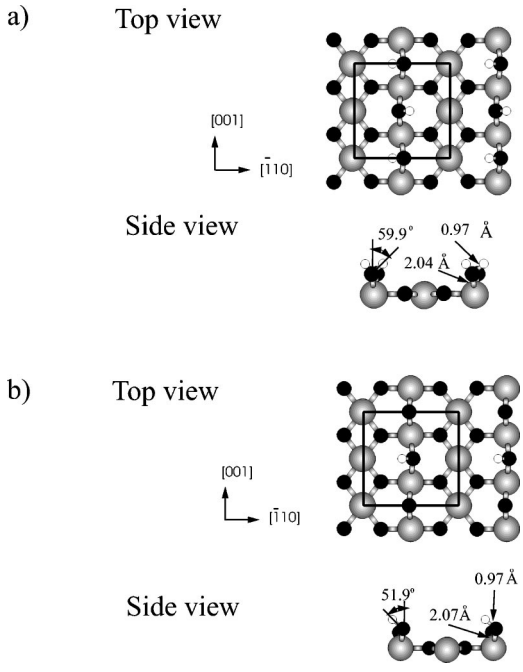


FIG. 7. (a) Top and side view of the adsorption geometry of 1 ML H at $O^{br}$, computed in $(1\times2)$ unit cells with alternating tilting. (b) Top and side view of the adsorption geometry of 0.5 ML H at $O^{br}$.

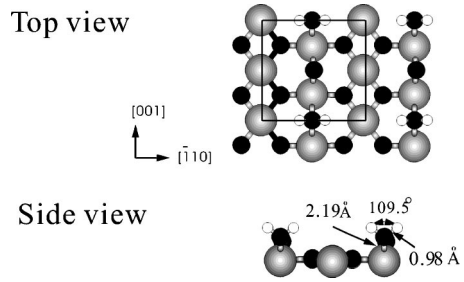


FIG. 8. Top and side view of the adsorption geometry of 0.5 ML waterlike species at the bridge sites, oriented along the $[\bar{1}10]$ direction.

the intramolecular bonds and normally widens the H—O—H angle, both these effects would rather tend to make the bending mode softer.[43] Trying to address this puzzling finding we computed such waterlike configurations at the bridge sites first at 1 ML $H_2O$-coverage in $(1\times1)$ cells and with the water-axis oriented once along [001] and once along $[\bar{1}10]$. Both configurations exhibit only a very low stability and can thus not account for the experimental waterlike species with a desorption temperature around 300 K.[18] We therefore proceeded to relax the same two configurations at lower coverages in $(1\times2)$ cells with waterlike species now only at every second bridge site. While the model with orientation along the [001] axis is still slightly endothermal, the binding energy of the other orientation shown in Fig. 8 finally turns out already at least exothermal by +0.48 eV/$H_2$. Still, as almost expected the calculated scissor mode for this configuration (just as much as the one of the other three models) is 168 meV significantly lower than the one of free water, and thus in strong disagreement with the experimental data.

Recalling the strong tilting of the monohydride group at $O^{br}$ shown in Fig. 5 we then tested to similarly tilt the whole waterlike species of the last most favorable model and ended up with the geometry shown in Fig. 9 that is apparently separated from the up-right configuration by a sizable energy barrier (i.e., neither configuration relaxes automatically into the other one). The tilt not only significantly increases the binding energy of this configuration by 0.08 eV to +0.56 eV/$H_2$, but also the computed scissor mode is 211 meV 12% higher than the one of a free water molecule (189 meV, see Table II). Also the other computed vibrational modes listed in Fig. 9(b) are now in reassuring agreement with the experimental HREELS data (exp: stretch 436 meV, scissor 231 meV, libration 110 meV 76 meV, translation 59 meV 28 meV).[18]

The question remains why this tilted geometry gives rise to the counterintuitively blueshifted scissor mode. Inspecting the relaxed geometry displayed in Fig. 9 in more detail we find the waterlike H—O—H bond angle with 108° slightly increased compared to free water (calculation: 103°, see Table II), lending more towards the argument favoring a weakening of the bending mode. However, this angle together with the overall tilting of the whole functional group causes the lower OH-bond of the waterlike species to end up almost parallel to the surface (only 8° to the surface plane),

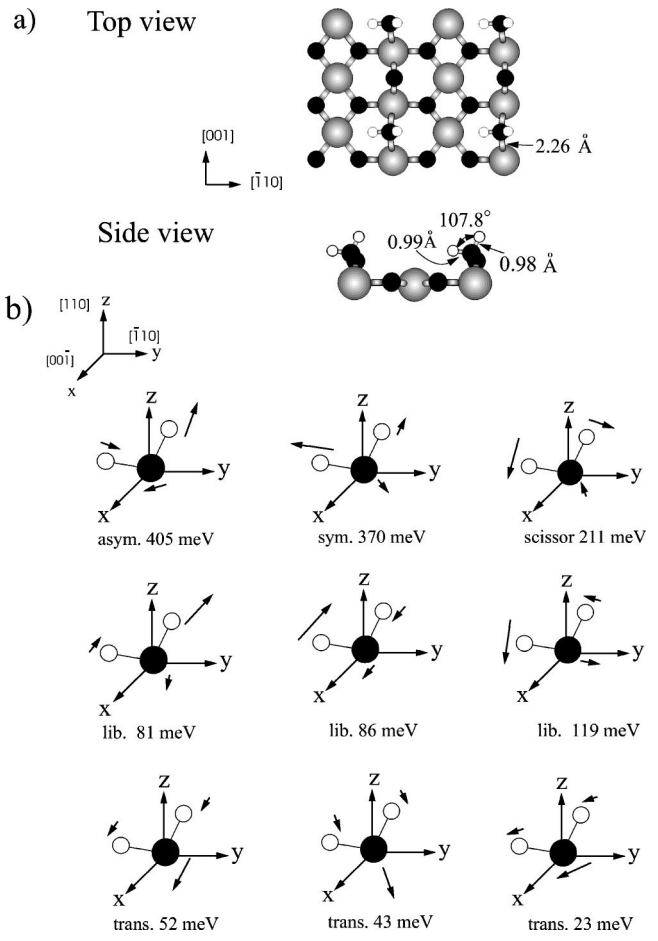


FIG. 9. (a) Top and side view of the adsorption geometry of 0.5 ML waterlike species at the bridge sites, oriented asymmetrically along the $[\bar{1}10]$ direction. (b) Corresponding nine vibrational modes.

bringing the terminal H atom closer to the neighboring $Ru^{cus}$ atom (2.72 Å compared to 3.19 Å in the upright model shown in Fig. 8). This suggests a possible interaction between these two species that is indeed verified by inspecting the computed difference density plot shown in Fig. 10. We interpret the well apparent polarization of the $Ru^{cus}$ and the H atom as a bonding possible in this tilted configuration. This hinders any movement away from $Ru^{cus}$ parallel to the $[\bar{1}10]$ direction and thus naturally stiffens not only the scissor mode, but also the corresponding librational mode (calc: 119 meV, exp: 110 meV, compared to "typical" values around 80 meV).

This intricate coupling between neighboring bridge and cus sites adds nicely to a first tentative picture of the low temperature dissociation kinetics of $H_2$ at $RuO_2(110)$ that emerges when combining the data presented in Secs. IV A and IV B with the data from the detailed UHV-HREELS experiments by Wang *et al.*[18] Although the thermodynamic ground state for hydrogen at this stoichiometric surface is given by the strongly bound hydroxyl-groups at the bridge sites (binding energy +0.89 eV/H atom),[16] direct dissociation over these sites is apparently inhibited at least at low temperatures by an energy barrier. The following scenario

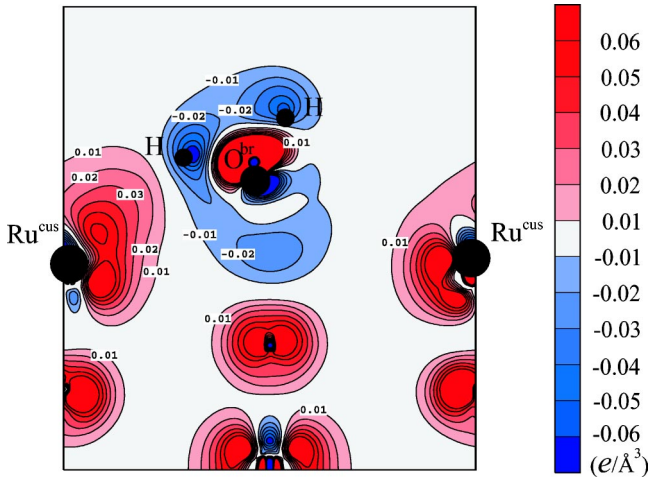


FIG. 10. Difference density plot of the asymmetric waterlike species of Fig. 9 at the bridge sites. The contour plot depicts the plane parallel to $[\bar{1}10]$ and normal to the surface. Areas of electron accumulation and depletion have positive and negative signs, respectively, contour lines are drawn at 0.01 $e$/Å$^3$ intervals.

would then be consistent with all available data: When $H_2$ interacts with $RuO_2(110)$, it is at first bound in molecular form at the cus sites (binding energy +0.16 eV/H atom). Although the $H_2$ bond is weakened in this process, the cus site does not induce its complete cleavage. This is instead achieved via the waterlike metastable configuration at the bridge sites (binding energy +0.28 eV/H atom) that may be accessed from the molecular $H_2$ state at the cus sites (as indicated by the low translational mode in the $[\bar{1}10]$ direction, cf. Fig. 3). From there the hydroxyl groups are finally formed, presumably by activated H diffusion. This interpretation of $H_2^{cus}$ as a necessary precursor state to dissociation is also supported by new low temperature HREELS and TDS experiments which report a suppressed population of the waterlike species at bridge if the cus sites are first blocked by CO molecules.[52] Only if the waterlike species are allowed to form, the hydroxyl groups result from moderate heating to 350 K.[18] While the sketched, intricate picture of the dissociation kinetics fits therefore all available experimental and theoretical data, we stress again that further calculations explicitly addressing the potential energy barriers combined with a full modeling of the kinetics and statistical mechanics between the here discussed (meta)stable configurations are necessary to really arrive at a conclusive understanding.

### C. Hydrogen at both sites: Higher coverages

Having discussed the lower coverage adsorption up to 1 $H_2$-ML for both sites separately, we now proceed to higher total coverages involving hydrogen at both sites. Also with various hydrogen functional groups present at the bridge sites we still find atomic hydrogen at cus to be always unstable. Correspondingly we restrict our detailed discussion to molecular $H_2$ at cus and different hydrogen populations at the bridge sites. Starting with the waterlike species at bridge, the $(1\times1)$ configuration $(H_2O)^{br}/H_2^{cus}$ corresponding to a to-

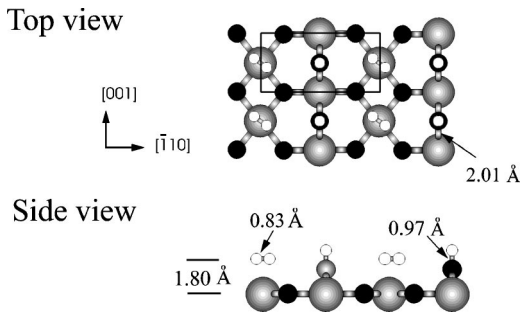


FIG. 11. Top and side view of the adsorption geometry of the 3 H-ML $(OH)^{br}/H_2^{cus}$ phase.

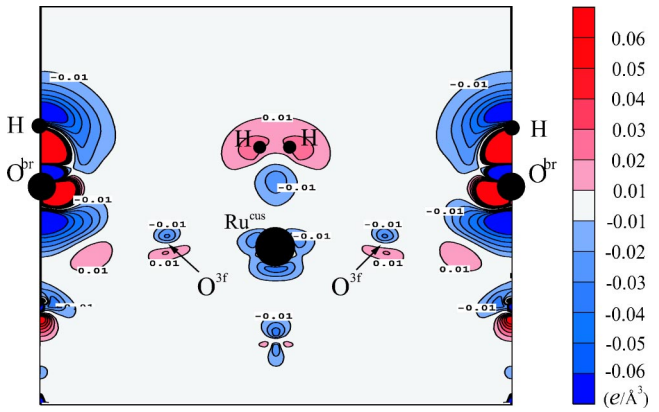


FIG. 12. Difference density plot of the high coverage $(1\times1)$ $(OH)^{br}/H_2^{cus}$ phase shown in Fig. 11. Displayed are the induced electron density changes in the system when hydrogen forms a hydroxyl group at the bridge sites. The contour plot depicts the plane normal to the surface that cuts through a bridge site and its next-nearest neighbor cus site (this way passing very close to a $O^{3f}$ atom and the positions which are nearest to the $O^{3f}$ are indicated by arrows). Areas of electron accumulation and depletion have positive and negative signs, respectively, contour lines are drawn at 0.01 $e$/Å$^3$ intervals.

tal coverage of 2 $H_2$-ML is computed to be endothermal, reflecting presumably already an oversaturation of the surface with hydrogen. This improves in more dilute $(1\times2)$ configurations with $(H_2O)^{br}$ and $H_2^{cus}$ occupying only every other site. The average binding energy for both a checkerboard arrangement and with both species occupying directly neighboring sites turns then out exothermic by about +0.2 eV/$H_2$, with a slight preference for the checkerboard arrangement in which the two hydrogen species maximize their mutual distance. This average binding energy is, however, still lower than the average binding energy we obtained for the $(1\times1)$ $O^{br}/H_2^{cus}$ phase (+0.32 eV/$H_2$, cf. Sec. IV A) which also corresponds to a total coverage of 1 $H_2$-ML.

This leaves as interesting higher coverage phase beyond 1 $H_2$-ML only the possibility to combine $H_2^{cus}$ with hydroxyl groups at the bridge sites. For this remaining combination even a dense $(1\times1)$ arrangement of $(OH)^{br}/H_2^{cus}$ at 1.5 $H_2$ -ML total coverage turns out very stable with an average binding energy of +0.6 eV/$H_2$. This points at the possibility that after the aforediscussed formation of hydroxyl groups at bridge also the molecular state at the cus sites could simultaneously be populated upon continued hydrogen uptake. In other words that the $RuO_2$(110) surface offers the fascinating property that hydrogen may coexist both in the dissociated monohydride and in the nondissociated dihydrogen state. Inspecting the corresponding geometry shown in Fig. 11, the first striking effect of the simultaneous occupation of bridge and cus states is that the pronounced tilting of the hydroxyl group, cf. Fig. 5, has disappeared. Next, the $H_2$ at the cus sites appears slightly more activated compared to the situation discussed in Sec. IV A when the bridging oxygen atoms were bare: The bond length is increased from 0.81 to 0.83Å, and the molecule resides at 1.80 Å height, i.e., 0.05 Å closer to the surface.

Interestingly, the formation of the hydroxyl group at the bridge sites seems to influence the bonding properties at the neighboring cus sites, rendering the latter somewhat more reactive. The mechanism with which this happens is nicely identified on the basis of the difference density plot shown in Fig. 12. Plotted are the induced electron density variations arising in the $(OH)^{br}/H_2^{cus}$ phase when the hydroxyl group is formed. Apart from the obvious significant density rearrangement at the bridge sites themselves [which is very similar to the one shown in Fig. 6 for the lower coverage $(OH)^{br}/-$ phase], also some variations can be observed at the distant cus sites: electron density is depleted around the $Ru^{cus}$ atoms and clearly populates the $H_2$ $\sigma^*$-orbital, thereby weakening the molecular bond. At the same time the $H_2$-metal bond is strengthened, so that the absolute binding energy is only slightly altered (0.23 eV/$H_2$ compared to the 0.32 eV/$H_2$ without the presence of the hydroxyl group, cf. Sec. IV A). Still, the molecule is more activated and adsorbs closer to the surface.

We interpret the surface's capability to give a higher backdonation to the cus-bond upon population of hydroxyl groups at bridge as arising from an interesting bond order propagation effect. Due to the newly formed hydroxyl bond the $O^{br}$ atoms become less bound to the underlying $Ru^{br}$ atoms, as reflected by the considerable increase in bond length from 1.91 to 2.01 Å. Having thus lost a bit of their optimum bonding environment, the $Ru^{br}$ seek to fortify their remaining back-bonds, among others also to the directly coordinated in-plane $O^{3f}$ atoms, cf. Fig. 2. The resulting electron density rearrangement at the latter atoms can nicely be discerned in Fig. 12, which displays a plane connecting next-nearest neighboring bridge and cus sites and thus passes also closely by the $O^{3f}$ sites. With this slightly strengthened bond to the $Ru^{br}$ atoms the $O^{3f}$ atoms in turn adapt by weakening their bonds to the $Ru^{cus}$ atoms. Due to this propagation of bond order the latter atoms find themselves in a neighborhood that is less electron demanding, allowing for an increased backdonation into the $H_2$-$Ru^{cus}$ bond.

The bonding properties at nearest-neighboring bridge and cus sites are thus obviously under a non-negligible mutual influence. This suggests that one could attempt to tune the reactivity of either site by a controlled population of the respective other site. Particularly for oxidation reactions at $RuO_2$(110) several studies have already emphasized the key role played by the cus sites.[6,9–11,13,15] Correspondingly, modifications at the bridge sites like the present decoration with

hydroxyl groups could have a noticeable impact on the overall catalytic activity of the surface, not only because of a possible site-blocking of bridge sites, but also because of an intricate tuning of the electronic structure at the cus sites. So far, all reaction mechanisms discussed at this $RuO_2(110)$ surface have been found to be initial-state dominated, i.e., the reaction barriers scaled with the binding energies of the adsorbed reactants.[7,13] The above described increased electron-donation ability of the cus sites upon hydroxylation of the bridge sites might therefore lead to a different reactivity of this oxide surface. Concomitantly we notice that a promoting effect of small amounts of hydrogen on the CO oxidation reaction over polycrystalline $RuO_2$ has already been reported in a recent experimental study, proposing this material as a suitable candidate for the technologically important low-temperature CO oxidation in humid air.[17] The present work identifies an increased reactivity of the cus sites after hydroxylation of the bridge sites at $RuO_2(110)$. Further work involving atom-specific surface science experiments on the reactivity of hydrogenated $RuO_2$ surfaces is now required to check if this can be exploited not only for total oxidation reactions, but possibly even more important for partial oxidation, where a controlled tuning of the reactive sites might be crucial to obtain a high selectivity.

## V. SUMMARY

In conclusion we presented a detailed DFT study of the energetic, electronic, structural, and vibrational properties of possible hydrogen states at the stoichiometric $RuO_2(110)$ termination. A different interaction with the two undercoordinated, prominent adsorption sites at this surface is found: At $Ru^{cus}$ only a molecular state can be stabilized, while the thermodynamic ground state is represented by hydroxyl groups involving the $O^{br}$ surface atoms. Combining our results with the detailed experimental HREELS and TPD data from the group of Jacobi and Ertl[18] suggests that low-temperature $H_2$ dissociation would require the molecular state at $Ru^{cus}$ as a precursor. We speculate that the low-temperature $H_2$ dissociation kinetics proceeds from the initial molecular adsorption at $Ru^{cus}$ first to a waterlike dihydride state at $O^{br}$, which exhibits a peculiar blueshifted scissor mode. This state can be accessed from the molecular state at $Ru^{cus}$, possibly by diffusion of the adsorbed $H_2$ molecule to the neighboring $O^{br}$ site. At increasing temperatures, activated H diffusion to neighboring still undecorated $O^{br}$ atoms leads then to the final hydroxyl groups.

Upon further hydrogen adsorption both the molecular $H_2$ state at the $Ru^{cus}$ site and the dissociated monohydride state at bridge-site surface oxygen atoms become populated. The formation of the hydroxyl groups is hereby found to intricately influence the reactivity at the neighboring cus sites, allowing for an increased backdonation further activating the $H_2^{cus}$ bond. This modification of the bonding properties at cus by hydrogen decoration at bridge is attributed to a bond order propagation mechanism, possibly special to this metallic oxide. It is argued that the resulting possibility of fine-tuning the cus site reactivity by controlled modification of the bridge site population could be of relevance for catalytic applications, in particular partial oxidation reactions where a precise tuning of the bond strengths could be crucial to obtain high selectivities.

TABLE III. Computed bond lengths ($d$ in Å), tilt angle (in deg), and absolute binding energies ($E_b$ in eV) as a function of interstitial plane wave cutoff and number of k-points in the irreducible part of the Brillouin zone for three phases characteristic for the present study.

| $O^{br}/-$ | $d_{O^{br}—Ru^{br}}$ | | | $E_b(O)$ |
|---|---|---|---|---|
| 20.25 Ry, 18 k | 1.91 | | | 2.54 |
| 25 Ry, 18 k | 1.90 | | | 2.46 |
| 25 Ry, 36 k | 1.90 | | | 2.43 |
| 30.25 Ry, 18 k | 1.91 | | | 2.43 |
| 36 Ry, 18 k | 1.91 | | | 2.37 |
| $(OH)^{br}/-$ | $d_{O^{br}—Ru^{br}}$ | $d_{H^{br}—O^{br}}$ | Tilt | $E_b(H)$ |
| 20.25 Ry, 18 k | 2.06 | 0.97 | 40 | 0.71 |
| 25 Ry, 18 k | 2.08 | 0.98 | 45 | 0.84 |
| 25 Ry, 36 k | 2.08 | 0.98 | 46 | 0.82 |
| 30.25 Ry, 18 k | 2.07 | 0.98 | 46 | 0.89 |
| 36 Ry, 18 k | 2.07 | 0.97 | 46 | 0.91 |
| $O^{br}/H_2^{cus}$ | $d_{O^{br}—Ru^{br}}$ | $d_{H—Ru^{cus}}$ | $d_{H—H}$ | $E_b(H_2)$ |
| 20.25 Ry, 18 k | 1.92 | 1.89 | 0.81 | 0.38 |
| 25 Ry, 18 k | 1.92 | 1.89 | 0.81 | 0.35 |
| 25 Ry, 36 k | 1.92 | 1.89 | 0.81 | 0.34 |
| 30.25 Ry, 18 k | 1.92 | 1.89 | 0.81 | 0.32 |
| 36 Ry, 18 k | 1.92 | 1.89 | 0.81 | 0.30 |

## ACKNOWLEDGMENTS

Q.S. is thankful for an Alexander von Humboldt fellowship. Valuable discussions with K. Jacobi, Y. Wang, J. Wang, C.Y. Fan, and G. Ertl are gratefully acknowledged.

## APPENDIX

In order to check on the numerical accuracy with respect to the finite basis set, we performed calculations with larger interstitital plane wave cutoffs and denser k-point meshes, the latter two being the most influential parameters in the FP-LAPW basis set. Specifically, we increased the cutoffs up to 36 Ry in several steps and doubled the k-point mesh in the $(1\times1)$ surface unit cells. Table III lists the resulting bond lengths, bond angles, and binding energies for three characteristic phases involved in the present study: the bare $RuO_2(110)$ surface ($O^{br}/-$), a hydroxyl-group at bridge [$(OH)^{br}/-$], and molecular hydrogen at cus ($O^{br}/H_2^{cus}$). It can be seen that the structural parameters of all three phases are well converged already at the lowest cutoff listed (20.25 Ry), with the exception of the hydroxyl group tilt angle in the $(OH)^{br}/-$ phase. We find the latter to be due to a very shallow structure of the potential energy surface (PES) minimum. As mentioned in Sec. IV B, it costs only 0.1 eV/H atom to reach the upright hydroxyl group position (i.e.,

change the angle by 40°). Converging such a flat part of the PES is hard, and correspondingly the change in angle with cutoff is a bit larger. We have carefully checked all other adsorption phases and find the corresponding PES minima to be much steeper with respect to the angular degrees of freedom (e.g., for the waterlike species at the bridge sites). Since also a doubling of the employed k-mesh has virtually no influence on the structural parameters, we conclude from these tests that bond lengths and bond angles should be converged to within 0.02 Å and 6°, respectively, already at the standard basis set with cutoff 20.25 Ry.

However, Table III shows that the absolute binding energies are not yet fully converged at this already quite demanding cutoff, primarily due to the need to use very small muffin-tin spheres as discussed in the text. From the convergence behavior along the sequence 20.25 Ry$\rightarrow$25 Ry $\rightarrow$30.25 Ry$\rightarrow$36 Ry we conclude that only at a high cutoff of 30.25 Ry at least the H bond energies are converged to within 0.1 eV/H atom. Fortunately, the relative energetic differences between similar geometries involving an equal number of O and H atoms appear to converge much more rapidly. At all tested cutoffs between 20.25 Ry and 36 Ry, we find, e.g., the binding energy of the hydroxyl group at bridge either in an upright or in the tilted configuration to exhibit an energetic difference of 0.1 eV/H atom, which remains constant to within 0.01 eV/H atom. Similar results were obtained when comparing the different tilt geometries in Figs. 5(a) and 7(a). Correspondingly, we employed the manageable cutoff of 20.25 Ry for structural relaxations, vibrational calculations, and when judging on the relative energetic sequence of similar structures. Only when absolute binding energies converged to within 0.1 eV/H atom are required did we run additional calculations at 30 Ry, but then with fixed geometry.


[1] V. E. Henrich and P. A. Cox, *The Surface Science of Metal Oxides* (Cambridge University Press, Cambridge, England, 1994).
[2] C. Noguera, *Physics and Chemistry at Oxide Surfaces* (Cambridge University Press, Cambridge, England, 1994).
[3] D. P. Woodruff and T. A. Delchar, *Modern Techniques of Surface Science* (Cambridge University Press, Cambridge, England, 1994).
[4] P. I. Sorantin and K. H. Schwarz, Inorg. Chem. **31**, 567 (1992).
[5] C. H. F. Peden and D. W. Goodman, J. Phys. Chem. **90**, 1360 (1986).
[6] H. Over, Y. D. Kim, A. P. Seitsonen, S. Wendt, E. Lundgren, M. Schmid, P. Varga, A. Morgante, and G. Ertl, Science **282**, 1474 (2000).
[7] H. Over and M. Muhler, Prog. Surf. Sci. **72**, 3 (2003).
[8] D. R. Rolison, P. L. Hagans, K. E. Swider, and J. W. Long, Langmuir **15**, 774 (1999).
[9] Y. D. Kim, A. P. Seitsonen, and H. Over, Surf. Sci. **465**, 1 (2000).
[10] C. Y. Fan, J. Wang, K. Jacobi, and G. Ertl, J. Chem. Phys. **114**, 10058 (2001).
[11] J. Wang, C. Y. Fan, K. Jacobi, and G. Ertl, Surf. Sci. **481**, 113 (2001); J. Chem. Phys. **106**, 3422 (2002).
[12] K. Reuter and M. Scheffler, Phys. Rev. B **65**, 035406 (2002).
[13] K. Reuter and M. Scheffler, Phys. Rev. B **68**, 045407 (2003).
[14] K. Reuter and M. Scheffler, Appl. Phys. A: Mater. Sci. Process. **78**, 793 (2004).
[15] K. Reuter and M. Scheffler, Phys. Rev. Lett. **90**, 046103 (2003).
[16] Q. Sun, K. Reuter, and M. Scheffler, Phys. Rev. B **67**, 205424 (2003).
[17] L. Zang and H. Kisch, Angew. Chem., Int. Ed. **39**, 3921 (2000).
[18] J. Wang, C. Y. Fan, Q. Sun, K. Reuter, K. Jacobi, M. Scheffler, and G. Ertl, Angew. Chem., Int. Ed. **42**, 2151 (2003).
[19] R. M. Dreizler and E. K. U. Gross, *Density Functional Theory* (Springer, Berlin, 1990).
[20] P. Blaha, K. Schwarz, and J. Luitz, WIEN97, *A Full Potential Linearized Augmented Plane Wave Package for Calculating Crystal Properites* (Techn. Universität Wien, Austria, 1999).
[21] B. Kohler, S. Wilke, M. Scheffler, R. Kouba, and C. Ambrosch-Draxl, Comput. Phys. Commun. **94**, 31 (1996).
[22] M. Petersen, F. Wagner, L. Hufnagel, M. Scheffler, P. Blaha, and K. Schwarz, Comput. Phys. Commun. **126**, 294 (2000).
[23] J. P. Perdew, K. Burke, and M. Ernzerhof, Phys. Rev. Lett. **77**, 3865 (1996).
[24] J. P. Perdew and Y. Wang, Phys. Rev. B **45**, 13 244 (1992).
[25] K. M. Glassford and J. R. Chelikowsky, Phys. Rev. B **47**, 1732 (1993).
[26] C. E. Boman, Acta Chem. Scand. (1947-1973) **24**, 116 (1970).
[27] Y. S. Huang, H. L. Park, and F. H. Plooak, Mater. Res. Bull. **17**, 241 (1982).
[28] Lj. Atanasoska, W. E. O'Grady, R. T. Atanasoski, and F. H. Pollok, Surf. Sci. **202**, 142 (1988).
[29] V. E. Henrich and R. L. Kurtz, Phys. Rev. B **23**, 6280 (1981).
[30] X.-G. Wang, A. Chaka, and M. Scheffler, Phys. Rev. Lett. **84**, 3650 (2000).
[31] *CRC Handbook of Chemistry and Physics*, 81st ed. (CRC Press, Boca Raton, FL, 2000).
[32] P. A. Thiel and T. E. Madey, Surf. Sci. Rep. **7**, 211 (1978).
[33] D. D. Wagman *et al.*, *NBS Chemical Thermodynamic Data Base* (National Bureau of Standards, Washington, DC, 1965).
[34] E. J. Baerends, M. Sodupe, and V. Brandachell, Chem. Phys. Lett. **265**, 481 (1997).
[35] E. Clementi and S. J. Chakravorty, J. Chem. Phys. **93**, 2591 (1990).
[36] B. Hammer and M. Scheffler, Phys. Rev. Lett. **74**, 3487 (1995).
[37] F. Finocchi and J. Goniakowski, Phys. Rev. B **64**, 125426 (2001).
[38] M. Ernzerhof and G. E. Scuseria, J. Chem. Phys. **110**, 5029 (1999).
[39] K. Reuter, D. Frenkel, and M. Scheffler, Phys. Rev. Lett. **93**, 116105 (2004).
[40] S. Wilke and M. Scheffler, Phys. Rev. B **53**, 4926 (1996).
[41] M. Gruyters and K. Jacobi, Chem. Phys. Lett. **225**, 309 (1994).
[42] M. Scheffler and C. Stampfl, in *Handbook of Surface Science, Vol. 2: Electronic Structure*, edited by K. Horn and M. Scheffler (Elsevier, Amsterdam, 2000).
[43] K. Christmann, Surf. Sci. Rep. **9**, 1 (1988).
[44] A. S. Martensson, C. Nyberg, and S. Andersson, Phys. Rev. Lett. **57**, 2045 (1986).

[45] P. K. Schmidt, K. Christmann, G. Kresse, J. Hafner, M. Lischka, and A. Gross, Phys. Rev. Lett. **87**, 096103 (2001).
[46] G. J. Kubas, R. R. Ryan, B. I. Swanson, P. J. Vergamini, and H. J. Wasserman, J. Am. Chem. Soc. **106**, 451 (1984).
[47] R. H. Crabtree and D. G. Hamilton, J. Am. Chem. Soc. **108**, 3124 (1986).
[48] G. J. Kubas, J. Less-Common Met. **172**, 475 (1991).
[49] K. W. Zilm, R. A. Merrill, M. W. Kummer, and G. J. Kubas, J. Am. Chem. Soc. **108**, 7837 (1986).
[50] L. S. van der Sluys, J. Eckert, O. Eisenstein, J. H. Hall, J. C. Huffman, S. A. Jackson, T. F. Koetzle, G. J. Kubas, P. J. Vergamini, and K. G. Caulon, J. Am. Chem. Soc. **112**, 4831 (1990).
[51] H. Brunner, *Applied Homogeneous Catalysis with Organometallic Compounds* (VCH, Weinheim, 1996).
[52] Y. Wang, J. Wang, C. Y. Fan, K. Jacobi, and G. Ertl (private communication).